Ab initio molecular dynamics calculations on reactions of molecules with metal surfaces

Nattino, F.

Chapter 6

Methane Dissociation on Pt(111): Searching for a Specific Reaction Parameter Density Functional

Abstract

The theoretical description of methane dissociating on metal surfaces is a current frontier in the field of gas-surface dynamics. Dynamical models that aim at achieving an highly accurate description of this reaction rely on potential energy surfaces based on density functional theory calculations at the generalized gradient approximation. We focus here on the effect that the exchange-correlation functional has on the reactivity of methane on a metal surface, using CHD_3 + Pt(111) as a test case. We present new *ab initio* molecular dynamics calculations performed with various density functionals, looking also at functionals that account for van der Waals (vdW) interactions. Results show that the use of a weighted average of the PBE and the RPBE exchange functionals together with a vdW-corrected correlation functional leads to good agreement with quantum state-resolved experimental data for the sticking probability.

6.1 Introduction

The level of accuracy that can be achieved in modeling gas-surface reaction dynamics strongly depends on the accuracy of the interaction potential employed. Assuming the Born-Oppenheimer approximation to be valid, the state-of-the-art electronic structure method that allows the computation of potential energy surfaces (PESs) for molecules interacting with metal surfaces is density functional theory (DFT) at the generalized gradient approximation (GGA) level [1]. However, many implementations of the GGA exist due to the unknown exchange-correlation functional (E_{XC}). Even though functionals at the GGA level are not expected to be accurate in predicting, for instance, the reaction barrier height for a given system (for gas phase reactions the lowest mean absolute error is 3.8 kcal/mol, as obtained with the MOHLYP2 functional [2, 3]), semi-empirical versions of E_{XC} allow one to produce accurate PESs through the fitting of one parameter to a single set of experimental data [4, 5].

Methane dissociation on metal surfaces is a reaction for which an accurate theoretical description has not yet been achieved. Many of the studies that focused on this system have been motivated by fundamental questions [6–27], but the reaction is also of industrial interest, as it is believed to represent a rate limiting step in the methane steam reforming process [28]. Mode specificity [11] with unusually large vibrational efficacies [12, 13], bond selectivity for the partially deuterated isotopologues [14, 21] and rotational alignment dependence [16, 29], are just a few examples of the interesting properties of the sticking probabilities that have been observed for this system.

We have previously shown (Ref. [30] and Chapter 5) that by using the PBE density functional [31,32] in combination with the *ab initio* molecular dynamics (AIMD) method, semi-quantitative agreement can be obtained with quantum state-resolved experimental sticking probabilities. The combination of the AIMD method and the system considered, CHD_3 + Pt(111), is suitable for testing the accuracy of the underlying PES. In fact, the quasi-classical trajectory technique can be used to accurately study the vibrational efficacy of the CH-stretch mode, as this vibrational mode is off-resonance with other modes due to the mass mismatch between the H and the heavier D atoms. Therefore, less

'artificial' intramolecular vibrational energy redistribution caused by the use of classical mechanics is expected for this isotopologue of methane in the case of pre-excitation of the CH-stretch mode [33]. Furthermore, by using the AIMD method no dynamical approximation with respect to the time evolution of any of the molecular degrees of freedom has to be made *a priori* [30,34] (see also Chapter 5). Moreover, the motion of the surface atoms, which has been shown to play a role in the dissociation dynamics of methane on metal surfaces [30,35], can be explicitly included in the dynamics.

The agreement with experimental data obtained using the PBE functional was limited (Ref. [30] and Chapter 5): The reactivity computed when simulating molecular beams in which the vibrational ground state is the most populated state ('laser-off' experiments) is overestimated. Furthermore, the vibrational efficacy obtained for the CH-stretch mode of CHD_3 is underestimated. In order to tackle these limitations, we present here a study of the influence of E_{XC} on the dissociation of methane on Pt(111). Our goal is to develop a semi-empirical density functional for this system, following the specific reaction parameter (SRP) approach. This approach, inspired by the work of Truhlar and coworkers [36,37], has been successfully applied to the reactive scattering of H_2 from low-index copper surfaces [4,5,38]. A SRP functional for this system, to be considered as such, must produce good agreement with the laser-off experimental reaction probabilities on the whole energy range for which data are available. Furthermore, it must predict the correct vibrational efficacy for the CH-stretch mode. We have considered various functionals, including functionals that mimic van der Waals (vdW) interactions [39], motivated by recent studies that demonstrated the improved description of two molecule-surface reactions achieved with vdW-corrected density functionals [40,41]. Note that the long ranged dispersion interactions are generally not described by traditional GGA functionals. First, we have investigated the presence of the vdW physisorption well that appears if a vdW-corrected correlation functional is employed. Secondly, static calculations have been performed to identify the minimum barrier height for each of the functionals considered. Finally, we present new AIMD calculations for CHD_3 dissociation on Pt(111), comparing the computed sticking probabilities to the previous

PBE-AIMD calculations and to the results of quantum state-resolved experiments [30].

The results indicate that the use of a density functional that employs the correlation functional of Dion et al. [39], which is able to mimic vdW-type interactions, and a weighted average of the PBE and the RPBE [42] exchange functionals, leads to improved agreement with experimental data. Surprisingly, this density functional returns a minimum barrier height that is equal to the PBE barrier height, suggesting that also other aspects of the PES affect the reactivity. The larger and improved vibrational efficacy obtained for the CH-stretch mode can be explained by invoking Polanyi's rule [43], according to which the more extended the dissociating CH bond is at the transition state, the higher should be the vibrational efficacy.

The structure of this chapter is as follows. In Section 6.2 the methodology is described. In Section 6.3, all the results are presented and discussed: Static calculations that focus on the vdW well (Section 6.3.1) and on the dissociation barrier (Section 6.3.2), and AIMD calculations (Section 6.3.3). Finally, the conclusions are presented in Section 6.4.

6.2 Methods

The sticking probability S_0 of methane on Pt(111) has been determined using the AIMD technique [44, 45]. Details about the calculations have been given previously (Ref. [30] and Chapter 5) and are only briefly summarized here. A (3x3)-surface-unit-cell slab with 5 atomic layers is employed to model the surface, and 13 Å of vacuum space have been used to separate periodic replicas of the surface. The bulk lattice constant as well as the interlayer distances have been self-consistently relaxed for each of the tested density functionals. The electronic structure calculations are characterized by an energy cutoff for the plane wave expansion equal to 350 eV. A Γ-centered 4x4x1 k-point grid has been employed to sample the first Brillouin zone, with the projector augmented wave (PAW) method [46, 47] to represent core electrons and a Fermi smearing with width parameter $\sigma = 0.1$ eV. All the calculations have been performed with the Vienna *ab initio* simulation package (VASP) [46,48–52]. In order to mimic surface temperature effects, the optimized

E_{XC}	a
PBE	3.975
RPBE	3.991
vdW-DF	4.032
optPBE-vdW	3.990
PBE-vdW	4.014
RPBE-vdW	4.039
RPBE:PBE/0.24:0.76	3.975
RPBE:PBE/0.1:0.9-vdW	4.017
Experimental	3.916

Table 6.1: Optimized lattice constants (in Å) for bulk Pt calculated using the various tested exchange-correlation functionals. The experimental value is from Refs. [53, 54].

lattice constants have been expanded according to experimental information [53, 54]. Note that for all the tested functionals, the optimized lattice constants (reported in Table 6.1) are in reasonable agreement with the experimental value of 3.916 Å [53, 54]. Displacements and velocities are initially assigned to the surface atoms to simulate their thermal motion, with exception of the atoms of the bottommost layers, which are kept fixed at their ideal positions. The procedure employed to sample the surface initial conditions is essentially the same as described in Ref. [30] and Chapter 5. To summarize, clean surface dynamical runs in which the number of particles in the simulation box, the volume and the total energy are kept constant (NVE runs), are employed to equilibrate ten surfaces at a specific surface temperature ($T_s = 120$ K and $T_s = 500$ K).

Between 500 and 2000 NVE trajectories have been computed to estimate S_0 for each molecular beam simulated. The initial conditions of the trajectories are chosen such that the velocity of the center of mass of the molecule samples the velocity distribution of the beam [55] determined by the experimentalists using time-of-flights (TOF) techniques (all beam parameters have been reported in Ref. [30] and Chapter 5). The angular momentum of the molecule is initially set to zero. Standard Monte Carlo techniques are employed to represent the initial vibrational state of the molecule, as already described in Ref. [30] and Chapter 5. We exploit the quasi-classical trajectory (QCT) method, which means that vibrational zero-point energy (ZPE) is initially imparted to the impinging molecules. With respect to our previous work, we have slightly modified

the operational definition of a reactive event. A trajectory is considered reacted if a CH or CD bond becomes larger than 2 Å and remains in this configuration for at least 100 fs, or, alternatively, if a CH or CD bond becomes larger than 3 Å. This operational definition accounts, at least in part, for the possibility of barrier recrossing. No considerable difference has been found if this definition of reactive event is applied to the previous PBE-AIMD calculations. A trajectory is considered scattered if the center of mass of the molecule reaches the distance of 6 Å from the surface, with the velocity pointing away from the surface. Error bars on the sticking probability values have been estimated using the Wilson method [56] and represent 95% confidence interval unless otherwise stated.

For what concerns the vibrational population of the supersonic molecular beams simulated, two types of beams have been considered. In the first type of beam, the vibrational ground state is the most populated state, but vibrationally exited molecules are also present due to collisions with a heated nozzle ('laser-off' beams). In order to simulate these beams, we have assumed the vibrational population to be Boltzmann-like with a vibrational temperature equal to the gas temperature. In the second class of beam, the CHD_3 molecules are selectively prepared with one quantum of vibration in the CH-stretch (ν_1) mode using a laser. Only molecules in the $\nu_1 = 1$ vibrational state have been used to simulate this second type of beam.

Two types of functional have been employed to represent the exchange-correlation functional in the electronic structure calculations. The first type of functional employed is characterized by PBE correlation [31, 32]. Apart from the PBE functional itself, we have considered the RPBE functional [42] and the use of a density functional that employs PBE correlation and an exchange functional of the following form:

$$E_X = x \cdot E_X^{RPBE} + (1 - x) \cdot E_X^{PBE}, \tag{6.1}$$

where E_X^{PBE} and E_X^{RPBE} are the PBE and the RPBE exchange functionals, respectively. The RPBE functional is known to be more repulsive than the PBE functional. By using a functional as in Equation 6.1 we can tune the barrier height of a system by changing

the value of the x coefficient [4, 5].

Wijzenbroek et al. [40] have recently shown that vdW-corrected density functionals improve the description of a molecule-surface reaction (H_2 + Ru(0001)). Moreover, vdW-corrected density functionals have been shown to better describe properties such as adsorption energy and reaction barriers for N_2 interacting with W(110), compared to traditional density functionals like PBE and RPBE. Motivated by these findings, the second class of functionals that we have tested is characterized by the non-local correlation functional proposed by Dion et al. [39] to mimic dispersion interactions (van der Waals forces), which are generally not correctly described with regular GGA functionals. Note that an efficient implementation of this non-local correlation functional has recently become available [52, 57]. This correlation functional (from now on vdW correlation) has been originally paired with revPBE [58] exchange, forming the so-called vdW-DF exchange-correlation functional [39], but it could in principle be used in combination with any exchange functional. In the current work, in addition to the vdW-DF functional, we have tested vdW correlation paired with PBE exchange (PBE-vdW), with RPBE exchange (RPBE-vdW), with optPBE exchange (optPBE-vdW) [59] and with an exchange functional of the form described by Equation 6.1. Note that the optPBE exchange functional is also defined as a weighted average of the PBE and the RPBE exchange expressions, with an addition modification of the κ and μ parameters which appear in both the PBE and the RPBE exchange functionals [59].

Barrier heights have been determined with climbing image nudged elastic band (CINEB) calculations, as implemented in the VASP transition state tools developed by Henkelman and Jónsson [60, 61]. Nave and Jackson explored different reaction paths for methane dissociating on Pt(111) [62, 63]. They identified the reaction pathway that leads to the adsorption of both the methyl group and the hydrogen atom on top sites as the path with the lowest energy transition state (TS). We have considered the same path for the CINEB calculations, optimizing four images between a methane molecule placed with its center of mass 4 Å far from the surface (the reactant state) and the dissociated configuration (the product state). The path has been optimized until all the

forces became smaller than 15 meV/Å. Note that for all the tested functionals the slab employed has been constructed using the optimized bulk lattice constant. Note also that the surface atoms have been kept fixed at their equilibrium positions during the CINEB calculations.

6.3 Results and Discussion

6.3.1 The Van der Waals Well

As mentioned earlier, regular GGA density functionals are known to fail at describing dispersion interactions. As a consequence, functionals like PBE or RPBE do not correctly model the physisorption of molecules on metal surfaces. Figure 6.1 A shows the interaction energy calculated as a function of the distance between the center of mass of CH_4 and an ideal Pt(111) slab (Z coordinate). The geometry of the molecule has been kept frozen at the optimized gas-phase configuration. The molecule is placed above the hcp hollow site with one hydrogen atom pointing away from the surface ($\theta = 0°$) and the other H atoms oriented toward the top sites. Note that the zero is defined as the energy of a methane molecule in its gas-phase relaxed geometry placed midway between two periodic replicas of the slab ($Z = 6.5$ Å). Using the PBE functional, only a shallow potential well that is about 20 meV deep is observed at $Z \approx 4$ Å. Using the vdW correlation functional that accounts for dispersion interactions, a considerably deeper adsorption well is obtained. As expected from the more repulsive nature of the RPBE exchange with respect to the PBE exchange, the vdW well calculated with the PBE-vdW functional is deeper and the minimum is slightly closer to the surface than for the RPBE-vdW functional. The energy profile for large Z, however, is very similar for the two vdW-corrected functionals: at $Z = 4.5$ Å the interaction energy calculated with the two functionals differs by only 10 meV, and this difference becomes even smaller at larger values of Z. This is consistent with the fact that the correlation functional only (the same for PBE-vdW and RPBE-vdW) is responsible for the interaction at the largest distances [39].

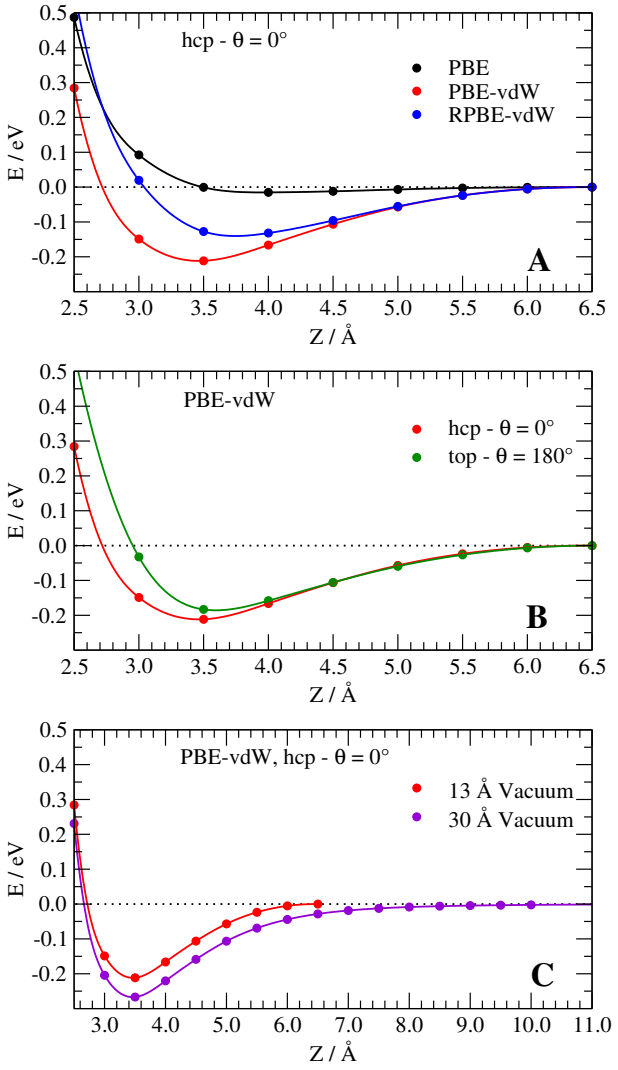

Figure 6.1: Interaction energy as a function of the distance of CH_4 from an ideal Pt(111) surface. We compare the energy profiles for three density functionals (A), for two molecular orientations and surface impact sites (B) and for two computational setups differing only in the amount of vacuum space between two periodic replicas of the slab (C).

In Figure 6.1 C we have plotted two 1D cuts of the PES calculated for the same molecular configuration chosen for Figure 6.1 A, using the PBE-vdW functional but employing different amounts of vacuum space between the slab and its periodic replica. The curve calculated with the setup characterized by the smaller vacuum space (13 Å) is shifted upwards by about 45 meV with respect to the other curve. For each computational setup the zero of the interaction energy is defined as the energy of a methane molecule in its gas-phase configuration placed midway between two periodic replicas of the slab. Note that for the system with 30 Å of vacuum space, at $Z = 6.0$ Å the interaction energy is about 45 meV. Therefore, the shift between the two curves is due to a residual attractive interaction for the gas-phase configuration of the setup with the smaller vacuum space. Unfortunately, the use of a larger vacuum space leads to an increase in the computational cost of the electronic structure calculations caused by the increased plane wave basis set size. Moreover, performing dynamics with the molecule initially placed at larger distances from the surface requires more time propagation steps for the molecule to reach the surface (and for the molecule to reach again the gas-phase after the impact with the surface, in the case of a scattering event). We have estimated that adding 3 Å of vacuum space to our computational setup would overall increase the computational cost of a scattered trajectory by about 50 %. On the other hand, using 13 Å of vacuum space affects the energetics by only a systematic 45 meV upward shift of the gas-phase level, while it allows to keep the computational cost relatively low. We only have to keep in mind that the presented values of adsorption energies and energy barriers calculated using the vdW correlation functional apply to the computational setup that we have employed, while with the use of a larger vacuum space the adsorption energies are expected to be about 45 meV larger and the barriers 45 meV lower.

In Figure 6.1 B we plot similar energy profiles as shown in Figure 6.1 A but for two different adsorption sites and molecular orientations. The functional employed is PBE-vdW. The two curves are only slightly different, and the biggest differences are observed at closer distances from the surface, suggesting that the multidimensional PES calculated using the vdW correlation functional is rather independent of X and Y, and of the

E_{XC}	E_{Ads}
PBE-vdW	0.214
RPBE-vdW	0.141
RPBE:PBE/0.1:0.9-vdW	0.205

Table 6.2: Adsorption energies (in eV) corresponding to the bottom of the van der Waals well calculated with various density functionals.

Euler angles of orientation in the proximity of the vdW (physisorption) well. We have optimized the molecular geometry testing various surface impact sites and molecular orientations and we have found that the configuration that corresponds to the minimum of the curves in Figure 6.1 A is the lowest in energy ($E_{ads} = 0.214$) while the adsorption energy differs by less than 43 meV if other molecular adsorption configurations (including other local minima) are considered. Note that for all the adsorption configurations considered the geometry of the molecule does not considerably differ from the gas-phase configuration. In Table 6.2 we report the molecular adsorption energy E_{ads} calculated with three different exchange correlation functionals: PBE-vdW, RPBE-vdW and a functional that employs the vdW correlation and the exchange of the form of Equation 6.1 with $x = 0.1$ (the choice of this value for the x coefficient will become clearer later on). Consistently with the curves reported in Figure 6.1 A, the adsorption energy calculated with the PBE-vdW functional is about 60 meV larger than the RPBE-vdW value, while the RPBE:PBE/0.1:0.9-vdW functional returns an intermediate value. As mentioned earlier in this section, these values of E_{ads} are expected to be about 45 meV larger for a computational setup with a larger amount of vacuum space.

Experimentally, methane is known to molecularly adsorb on Pt(111) with an adsorption energy in the range 0.17 eV - 0.23 eV [64–68]. The values of E_{Ads} reported in Table 6.2 are in fairly good agreement with this experimental range. Considering the extra 45 meV that would have to be added when considering a larger vacuum space, the PBE-vdW and the RPBE:PBE/0.1:0.9-vdW functionals would slightly overestimate the adsorption energy, while the adsorption energy calculated with the RPBE-vdW functional would fall inside the experimental range.

We note in passing that accurately modeling the vdW well for methane interacting

with metal surfaces would be relevant for describing two recent sets of experimental data [69, 70]. In a first study, the Beck's group focused on the effect that vibrational excitation has on the physisorption probability of CH_4 and on the dissociation probability of CH_4 physisorbed on Pt(111) [69]. In a second study, Utz and coworkers, suggested a precursor-mediated dissociation channel for CH_4 impinging at very low collision energies on Ir(111) [70]. To our knowledge all dynamical studies that have appeared so far relied on density functionals that fail at modeling dispersion interactions, and therefore cannot be used to model these two sets of experimental data.

6.3.2 The Dissociation Barrier

Using CINEB calculations, we have identified the TS along a reaction path that connects a molecule in its equilibrium geometry placed at $Z = 4$ Å to a dissociated configuration corresponding to a methyl fragment and a hydrogen atom adsorbed on two neighboring top sites with one CH bond of the methyl group pointing toward the adsorbed H. This path, illustrated in Figure 6.2, has been suggested by Nave et al. to correspond to the minimum energy path for dissociation for CH_4 on Pt(111) [63]. In Figure 6.2 we plot the energy computed along the dissociation path for the various tested functionals. Note that the density functionals that account for vdW interactions predict negative energies on the reactant side of the barrier, as expected from the presence of a vdW well (see Section 6.3.1). Product energies also can vary significantly, and the dissociation path considered is predicted to be endothermic or slightly exothermic depending on the functional employed.

Some details about the TSs obtained are summarized in Table 6.3, where we report the TS energy (with and without zero-point energy corrections) and some descriptors of the TS geometry: the distance of the C atom to the surface Z_C, the distance of the dissociating H atom to the surface Z_H, the angle included between the dissociating CH bond and the surface normal θ_{diss}, and the length of the dissociating CH bond, r_b. Note again that the TS energies calculated using the vdW correlation functional are expected to be about 45 meV larger for computational setups including a larger amount of vacuum

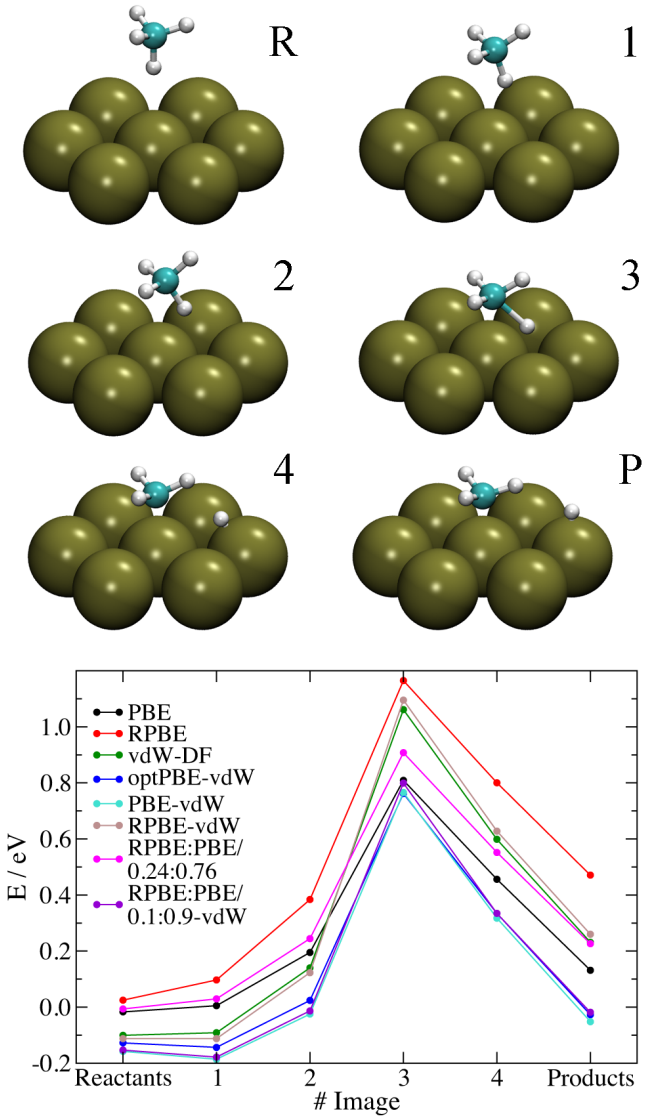

Figure 6.2: Above: Illustration of the molecular configurations that correspond to the images resulting from CINEB calculations. Below: The energy of each image is plotted as a function of the image number (R and P are for reactants and products, respectively). The colors distinguish the various density functionals (lines are for guiding the eye).

E_{XC}	E_b (E_b^c)	Z_C	Z_H	θ_{diss}	r_b
PBE	0.809 (0.687)	2.251	1.213	133.8	1.500
RPBE	1.165 (1.042)	2.274	1.218	133.5	1.534
vdW-DF	1.061 (0.942)	2.307	1.220	134.0	1.566
optPBE-vdW	0.762 (0.638)	2.278	1.224	133.5	1.531
PBE-vdW	0.766 (0.643)	2.286	1.217	133.9	1.541
RPBE-vdW	1.096 (0.976)	2.313	1.219	134.1	1.572
RPBE:PBE/0.24:0.76	0.908 (0.785)	2.257	1.222	133.2	1.512
RPBE:PBE/0.1:0.9-vdW	0.799 (0.679)	2.288	1.225	133.3	1.550

Table 6.3: Transition state properties calculated with various density functionals for CH_4 reacting on Pt(111). E_b^c and E_b are the minimum barrier heights with and without zero-point energy corrections (in eV), Z_C and Z_H are the distance to the surface of the C atom and of the dissociating H atom (in Å), respectively, θ_{diss} is the angle included between the dissociating CH bond and the surface normal (in degrees) and r_b is the length of the dissociating CH bond at the transition state (in Å).

space between periodic replicas of the slab (see Section 6.3.1).

We observe that the geometries of the TSs identified do not differ considerably in the values of θ_{diss} and Z_H, while Z_C and r_b are the most affected by the choice of the density functional employed. We also observe that ZPE corrections affect the barrier heights with a shift downwards of about 0.12 eV, independent of the density functional employed. In the case of a different isotopologue of methane, like CHD_3, slightly different ZPE corrections may apply, which would also depend on whether a CH bond or a CD bond is dissociating. However, we expect these corrections to be the same for all the functionals, and therefore they would not affect the comparison between the functionals.

The TS geometry that we have found using the PBE functional is very similar in the values of Z_C, Z_H, θ_{diss} and r_b to the barrier geometry found by Nave et al. [63]. Small differences could be expected from the different computational setups (surface unit cell size, number of atomic layers, cutoff energy, k-point grid). The TS energy that we have found, however, is about 0.12 eV lower than the value of Ref. [63]. This difference can be explained accounting for the different surface unit cell size and the different number of atomic layers, as already shown in our previous work [30, 34] (see also Chapter 5).

The overestimation of the laser-off reactivity using the PBE functional made us conclude that the PBE functional underestimates the dissociation barrier by about 0.1 eV (Ref. [30] and Chapter 5). A popular density functional that is known to produce

higher reaction barriers is the RPBE functional. Viñes et al. [71] reported a TS energy of 1.06 eV for the RPBE functional and a computational setup similar to the one that we have used. Here, we have also obtained a larger E_b value for the RPBE functional (about 1.17 eV, see Table 6.3). The discrepancy could be explained if the barrier reported in Ref. [71] would include surface relaxation effects, which is not explicitly mentioned. In fact, the upward motion of the surface atom below the dissociating molecule has been shown to be able to lower the barrier by up to 0.15 eV for this system [63].

The barrier that we have computed using the RPBE functional is about 0.36 eV larger than the PBE barrier, as expected from the more repulsive nature of the former with respect to the latter. Considering the 0.1 eV energy shift between the experimental reaction probability curve and the PBE simulations, we expect the RPBE functional to highly overestimate the barrier height for this system. We note in passing that the RPBE barrier is slightly 'later' than the PBE barrier, with r_b being about 35 mÅ more elongated. Calculations employing the PBE correlation together with an exchange functional of the form of Equation 6.1 with a mixing coefficient $x = 0.24$, have produced a barrier of 0.91 eV (see Table 6.3), approximately 0.1 eV larger than the E_b value obtained with the PBE functional.

Table 6.3 also includes the results of CINEB calculations performed with various density functionals that employ vdW correlation. The originally proposed vdW-DF density functional, which exploits revPBE [58] exchange, returns a TS energy which is similar to the one obtained using the RPBE-vdW functional (35 meV difference). Similarly, the optPBE-vdW and the PBE-vdW functionals produce almost identical barrier heights (4 meV difference). We note that the TS energy calculated using the PBE-vdW (RPBE-vdW) functional is lower than the corresponding PBE (RPBE) value. Surprisingly, dynamics performed using the PBE-vdW functional returned a laser-off reactivity slightly lower than the PBE one, but still overestimating the experimental values. By mixing PBE exchange with more repulsive RPBE exchange (mixing coefficient $x = 0.1$) we obtain a barrier which is about 35 meV larger than the PBE-vdW value. Note that the TS states obtained using the PBE-vdW and the RPBE-vdW functionals are charac-

terized by somewhat larger r_b values compared to the PBE and the RPBE functionals, respectively.

6.3.3 The Sticking Probability

We have previously shown (Ref. [30] and Chapter 5) that the sticking probability S_0 calculated for CHD_3 on Pt(111) using AIMD in combination with the PBE functional gave semi-quantitative agreement with experimental data (see also Figure 6.3 A). The discrepancies between theory and experiment can be summarized in three points: (i) the PBE-AIMD calculations overestimate the experimental laser-off reaction probability; (ii) the PBE-AIMD reaction probability increases too steeply with increasing collision energy; (iii) the energy shift between the PBE-AIMD CH-stretch excited and laser-off reaction probability curves (i.e. the vibrational efficacy of the CH-stretch mode) is too small compared to experiment.

In order to address point (i), we have performed AIMD calculations using the RPBE:PBE/0.24:0.76 density functional. The energy shift between the PBE laser-off sticking probability points and the experimental data at the lowest collision energies simulated is about 0.1 eV, just like 0.1 eV is the energy difference between the RPBE:PBE/0.24:0.76 and the PBE minimum barrier heights (see Section 6.3.2). Results are plotted in Figure 6.3 A and Figure 6.4 A, together with the PBE-AIMD results and the experimental data. As expected from the larger energy barrier, the reaction probability computed with the RPBE:PBE/0.24:0.76 functional is lower than the PBE one for all the collision energies. Very good agreement with experimental data is obtained for the laser-off beams at the lowest collision energies. The laser-off reactivity at the highest collision energies simulated is only slightly lowered compared to PBE results. The small relative change in S_0 is presumably due to the fact that the translational energy is so much in excess of the minimum energy barrier that the dynamics is not much affected by a 0.1 eV difference in the barrier height. The use of the RPBE:PBE/0.24:0.76 functional, however, dramatically affects the reactivity of the CH-stretch excited beams, and the computed reaction probability falls considerably below the experimental values

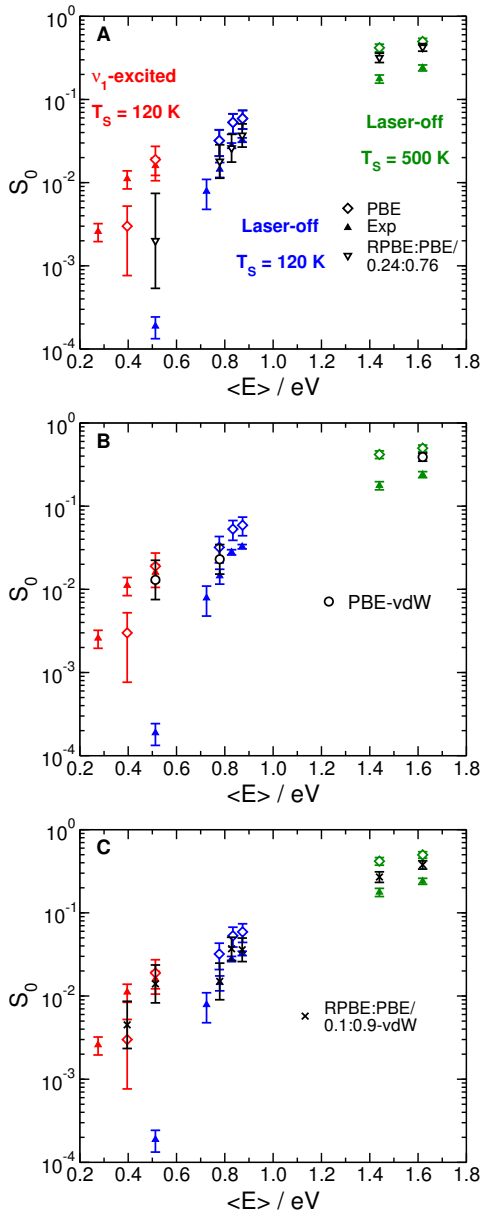

Figure 6.3: Dissociation probability as a function of the average collision energy for CHD_3 on Pt(111). Experimental data are compared to AIMD calculations performed with various exchange-correlation functionals.

when using this functional.

In Figure 6.5 A we plot the projection of the center of mass on the surface unit cell for all the molecules that go on to react, as computed with the PBE functional for the largest collision energy considered ($\langle E_i \rangle = 1.54$ eV). Reaction clearly occurs all over the surface unit cell, and is not limited to the top site (i.e. the minimum energy barrier impact site [62, 63]), in contrast to what was observed at lower collision energies (Ref. [30] and Chapter 5). Consistently, the impact parameter distribution, i.e., the distribution of the lateral displacements between the center of mass of the reacting molecules and the closest first layer Pt atom, is very broad (Figure 6.5 C). A possible explanation for the too steep increase in the PBE-AIMD reaction probability curve (point (ii)), which is not solved by the RPBE:PBE/0.24:0.76 density functional, could be that the PES corrugation is not correctly described by the PBE (and RPBE:PBE/0.24:0.76) functional: if the energy difference between the minimum barrier height and the barrier heights at other surface sites would be larger, the reaction probability would increase less rapidly with incidence energy.

Density functionals that account for dispersion interactions have been recently shown to produce broader reaction probability curves for H_2 on Ru(0001) [40]. In order to verify whether this finding also applies to our system of interest, we have calculated S_0 for CHD_3 on Pt(111) using the PBE-vdW functional. Due to the computational cost of the method, we have computed only three sticking probability points using this functional. The three points chosen are representative of the laser-off reactivity on the large range of collision energies studied and of the two vibrational state populations considered. Surprisingly, even though the minimum energy barrier calculated for the PBE-vdW functional is about 40 meV lower than the PBE energy barrier (see Table 6.3), the reaction probability calculated with the PBE-vdW functional is lower than for PBE in all cases (see Figure 6.3 B and Figure 6.4 B). In particular, the PBE-vdW laser-off reactivity agrees with the experimental data at the lowest collision energy simulated to within the experimental and calculated error bars, and S_0 is decreased with respect to the PBE value by about 10% at the highest collision energy. The reactivity

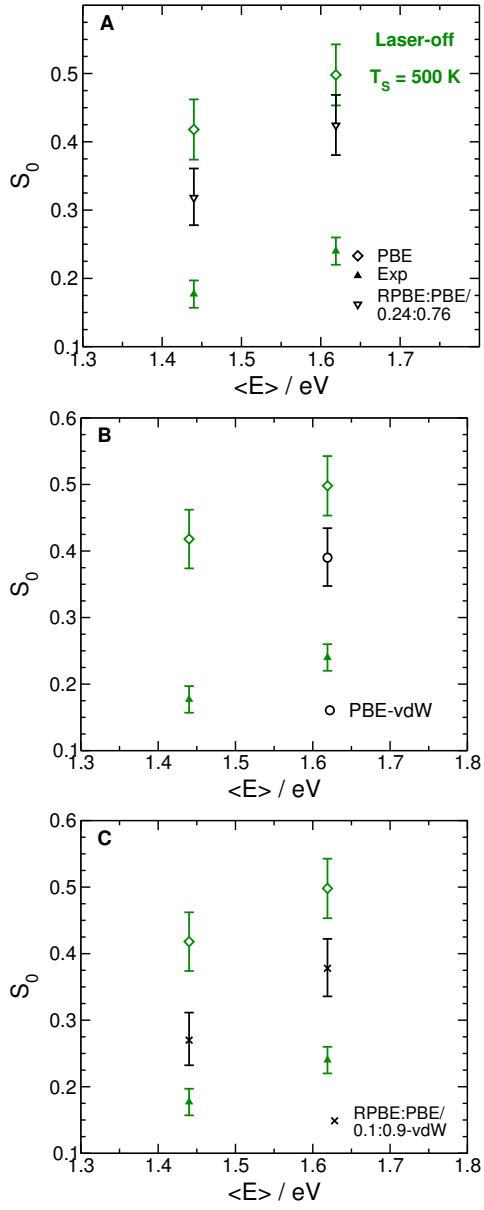

Figure 6.4: Same as Figure 6.3, but the focus is on the highest energy points and the sticking probability is plotted on a linear scale.

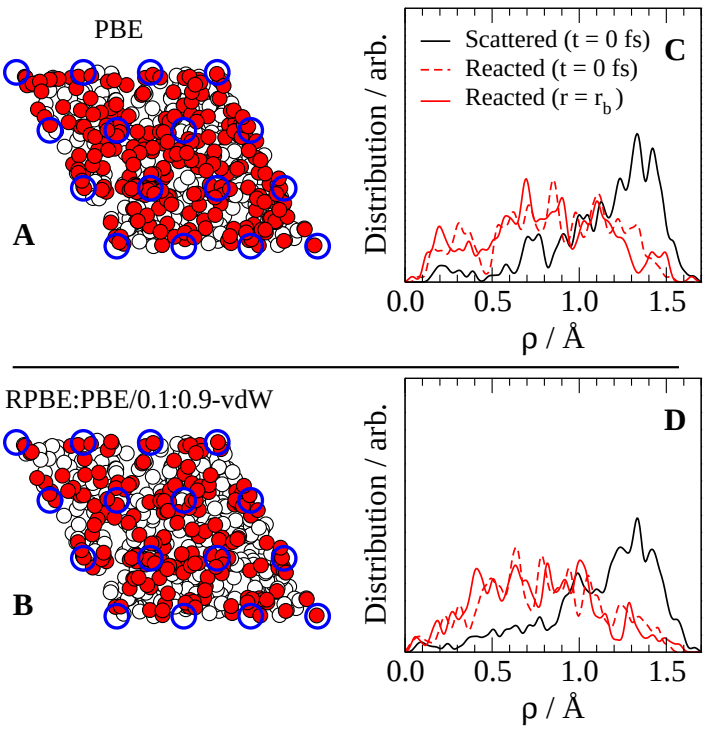

Figure 6.5: A and B: Bird-eye view of the initial center of mass positions of all the simulated molecules. Reacting and scattered molecules are plotted as red and white dots, respectively. The blue circles represent the first layer Pt atoms in their equilibrium positions. C and D: Lateral displacement distributions calculated between the center of mass of the molecule and the closest first layer Pt atom (impact parameter ρ). The initial distribution and the distribution calculated at the transition state for the reacting molecules are plotted as a dashed and a solid red lines, respectively. The initial distribution calculated for scattered molecules is plotted as a solid black line. All data refer to CHD_3 on Pt(111) at $T_s = 500$ K and $\langle E_i \rangle = 1.54$ eV.

obtained simulating a CH-stretch excited molecular beam is only slightly affected, and the agreement with experimental data is still good.

If we use an exchange of the form of Equation 6.1, with a mixing coefficient $x = 0.1$ in combination with the vdW correlation (RPBE:PBE/0.1:0.9-vdW functional), we obtain a slightly lower laser-off reactivity compared to the PBE-vdW functional (see Figure 6.3 C), which is consistent with a slightly higher dissociation barrier for the former (see Table 6.3). The agreement with the experimental data is thereby further improved. At the highest collision energies considered, theory still overestimates the experimental data (see Figure 6.4 C), but the discrepancy is reduced with respect to PBE calculations.

However, it is not completely clear why the PBE-vdW and the RPBE:PBE/0.1:0.9-vdW functionals return lower reactivity than the PBE functional. At the highest collision energy, in fact, the RPBE:PBE/0.1:0.9-vdW functional returns as broad an impact parameter distribution as the PBE functional (Figure 6.5 D). Therefore, the reason seems not to lie in an increased PES corrugation in the degrees of freedom corresponding to the lateral motion of the molecule (X and Y). Similarly, θ and ϕ distributions computed with the PBE and the RPBE:PBE/0.1:0.9-vdW functionals for the reactive molecules seem to be equally broad (not shown). The reason for the lower reactivity of the RPBE:PBE/0.1:0.9-vdW functional could lie in a somewhat more difficult access to the TS due to, for instance, the more elongated CH bond at the TS (see Table 6.3). Most notably, by using the RPBE:PBE/0.1:0.9-vdW functional, we obtain a good description of the reactivity for the CH-stretch excited beams. Considering the improved agreement for both laser-off and CH-stretch excited conditions, we conclude that the proposed functional better describes the vibrational efficacy of the CH-stretch mode than the PBE functional (point (iii)). An explanation for this is that the TS is slightly 'later', since the dissociating CH bond is 50 mÅ more elongated than with the PBE functional. According to Polanyi's rule [43] vibrational excitation should then be more effective in enhancing reactivity.

Considering the discrepancy still present between the simulated and the experimental reactivity of the laser-off beams at the highest collision energies, we consider the aim of obtaining a SRP density functional for methane reacting on Pt(111) not yet achieved with the RPBE:PBE/0.1:0.9-vdW functional. Our work suggests that a good functional for this system should exhibit a larger energetic corrugation than the PBE and the RPBE:PBE/0.1:0.9-vdW functionals. Other functionals that account for vdW interactions, like the vdW-DF2 [72], could be tested for this purpose.

As a final note, we mention again that the level of agreement obtained with experimental data using AIMD in combination with the RPBE:PBE/0.1:0.9-vdW functional, is expected to depend on the computational setup employed in the sense that this functional would return a barrier about 45 meV lower when using a larger amount

of vacuum space (see Section 6.3.1). However, we expect that by adjusting the mixing coefficient towards a larger percentage of RPBE exchange, the same level of agreement with experimental data could be obtained. This might even improve the description of the CH-stretch excited molecular beam reactivity further, as the barrier will become slightly later (larger r_b at the TS), consequently increasing the efficacy of the CH-stretch vibrational mode in promoting the reactivity.

6.4 Summary and Conclusions

We have tested the influence of the exchange-correlation functional E_{XC} on the reactivity of methane on a platinum surface, using the dissociation of the CHD_3 isotopologue on Pt(111) as a test case. Dynamical calculations have been performed using the AIMD technique, which is ideal for the purpose of testing the influence of E_{XC} on the sticking probability. In fact, the AIMD method allows the calculation of statistically accurate dissociation probabilities without the need of introducing *a priori* dynamical approximations concerning the evolution of specific molecular degrees of freedom or concerning the role played by surface atom motion. The computed sticking probabilities have been compared to recent quantum state-resolved experimental data and to previous calculations performed using the PBE density functional (Ref. [30] and Chapter 5). Calculations reveal that a density functional that returns a minimum barrier height 0.1 eV larger than the PBE functional (RPBE:PBE/0.24:0.76) improves the agreement with laser-off experimental data at the lowest collision energies simulated, but only slight improvement is observed at the high collision energies, and the agreement is drastically worsened for CH-stretch excited beams. The overall best agreement is observed for a density functional consisting of the correlation functional of Dion et al. [39], developed to mimic vdW interactions, and a linear combination of the RPBE and PBE exchange functionals (the RPBE:PBE/0.1:0.9-vdW functional). This functional still returns a too high reaction probability when simulating the high collision energy laser-off molecular beams, but for the lower collision energies the agreement with the experimental data is good. Surprisingly, the barrier height that this functional returns is the same as for the

PBE functional, so that the lower reactivity of the laser-off RPBE:PBE/0.1:0.9-vdW functional should be due to other aspects of the PES. The improved (larger) vibrational efficacy of the CH-stretch mode obtained with the RPBE:PBE/0.1:0.9-vdW functional is most likely due to the more elongated dissociating CH bond at the TS obtained with this functional.

Bibliography

[1] G. J. Kroes, Phys. Chem. Chem. Phys. **14**, 14966 (2012).

[2] R. Peverati and D. G. Truhlar, Phil. Trans. R. Soc. A **372**, 20120476 (2014).

[3] J. Zheng, Y. Zhao, and D. G. Truhlar, J. Chem. Theory Comput. **5**, 808 (2009).

[4] C. Díaz, E. Pijper, R. A. Olsen, H. F. Busnengo, D. J. Auerbach, and G. J. Kroes, Science **326**, 832 (2009).

[5] C. Díaz, R. A. Olsen, D. J. Auerbach, and G. J. Kroes, Phys. Chem. Chem. Phys. **12**, 6499 (2010).

[6] C. T. Rettner, H. E. Pfnür, and D. J. Auerbach, J. Chem. Phys. **84**, 4163 (1986).

[7] A. C. Luntz and D. S. Bethune, J. Chem. Phys. **90**, 1274 (1989).

[8] L. B. F. Juurlink, P. R. McCabe, R. R. Smith, C. L. DiCologero, and A. L. Utz, Phys. Rev. Lett. **83**, 868 (1999).

[9] J. Higgins, A. Conjusteau, G. Scoles, and S. L. Bernasek, J. Chem. Phys. **114**, 5277 (2001).

[10] L. Halonen, S. L. Bernasek, and D. J. Nesbitt, J. Chem. Phys. **115**, 5611 (2001).

[11] R. D. Beck, P. Maroni, D. C. Papageorgopoulos, T. T. Dang, M. P. Schmid, and T. R. Rizzo, Science **302**, 98 (2003).

[12] R. R. Smith, D. R. Killelea, D. F. DelSesto, and A. L. Utz, Science **304**, 992 (2004).

[13] P. Maroni, D. C. Papageorgopoulos, M. Sacchi, T. T. Dang, R. D. Beck, and T. R. Rizzo, Phys. Rev. Lett. **94**, 246104 (2005).

[14] D. R. Killelea, V. L. Campbell, N. S. Shuman, and A. L. Utz, Science **319**, 790 (2008).

[15] L. B. F. Juurlink, D. R. Killelea, and A. L. Utz, Prog. Surf. Sci. **84**, 69 (2009).

[16] B. L. Yoder, R. Bisson, and R. D. Beck, Science **329**, 553 (2010).

[17] M. Sacchi, D. J. Wales, and S. J. Jenkins, J. Phys. Chem. C **115**, 21832 (2011).

[18] B. Jackson and S. Nave, J. Chem. Phys. **135**, 114701 (2011).

[19] M. Sacchi, D. J. Wales, and S. J. Jenkins, Phys. Chem. Chem. Phys. **14**, 15879 (2012).

[20] M. Sacchi, D. J. Wales, and S. J. Jenkins, Comput. Theor. Chem. **990**, 144 (2012).

[21] L. Chen, H. Ueta, R. Bisson, and R. D. Beck, Faraday Discuss. **157**, 285 (2012).

[22] B. Jiang and H. Guo, J. Phys. Chem. C **117**, 16127 (2013).

[23] B. Jiang, R. Liu, J. Li, D. Xie, M. Yang, and H. Guo, Chem. Sci. **4**, 3249 (2013).

[24] S. B. Donald, J. K. Navin, and I. Harrison, J. Chem. Phys. **139**, 214707 (2013).

[25] M. Mastromatteo and B. Jackson, J. Chem. Phys. **139**, 194701 (2013).

[26] B. Jackson and S. Nave, J. Chem. Phys. **138**, 174705 (2013).

[27] X. J. Shen, A. Lozano, W. Dong, H. F. Busnengo, and X. H. Yan, Phys. Rev. Lett. **112**, 046101 (2014).

[28] G. Jones, J. G. Jakobsen, S. S. Shim, J. Kleis, M. P. Andersson, J. Rossmeisl, F. Abild-Pedersen, T. Bligaard, S. Helveg, B. Hinnemann, J. R. Rostrup-Nielsen, I. Chorkendorff, J. Sehested, and J. K. Nørskov, J. Catal. **259**, 147 (2008).

[29] B. L. Yoder, R. Bisson, P. M. Hundt, and R. D. Beck, J. Chem. Phys. **135**, 224703 (2011).

[30] F. Nattino, H. Ueta, H. Chadwick, M. E. van Reijzen, R. D. Beck, B. Jackson, M. C. van Hemert, and G. J. Kroes, J. Phys. Chem. Lett. **5**, 1294 (2014).

[31] J. P. Perdew, K. Burke, and M. Ernzerhof, Phys. Rev. Lett. **77**, 3865 (1996).

[32] J. P. Perdew, K. Burke, and M. Ernzerhof, Phys. Rev. Lett. **78**, 1396 (1997).

[33] Z. Xie, J. M. Bowman, and X. Zhang, J. Chem. Phys. **125**, 133120 (2006).

[34] B. Jackson, F. Nattino, and G. J. Kroes, J. Chem. Phys. **141**, 054102 (2014).

[35] A. K. Tiwari, S. Nave, and B. Jackson, J. Chem. Phys. **132**, 134702 (2010).

[36] Y. Y. Chuang, M. L. Radhakrishnan, P. L. Fast, C. J. Cramer, and D. G. Truhlar, J. Phys. Chem. A **103**, 4893 (1999).

[37] A. Chakraborty, Y. Zhao, H. Lin, and D. G. Truhlar, J. Chem. Phys. **124**, 044315 (2006).

[38] L. Sementa, M. Wijzenbroek, B. J. van Kolck, M. F. Somers, A. Al-Halabi, H. F. Busnengo, R. A. Olsen, G. J. Kroes, M. Rutkowski, C. Thewes, N. F. Kleimeier, and H. Zacharias, J. Chem. Phys. **138**, 044708 (2013).

[39] M. Dion, H. Rydberg, E. Schröder, D. C. Langreth, and B. I. Lundqvist, Phys. Rev. Lett. **92**, 246401 (2004).

[40] M. Wijzenbroek and G. J. Kroes, J. Chem. Phys. **140**, 084702 (2014).

[41] L. Martin-Gondre, J. I. Juaristi, M. Blanco-Rey, R. Díez Muiño, and M. Alducin, J. Chem. Phys. **142**, 074704 (2015).

[42] B. Hammer, L. B. Hansen, and J. K. Nørskov, Phys. Rev. B **59**, 7413 (1999).

[43] J. C. Polanyi, Acc. Chem. Rev. **5**, 161 (1972).

[44] A. Groß and A. Dianat, Phys. Rev. Lett. **98**, 206107 (2007).

[45] F. Nattino, C. Díaz, B. Jackson, and G. J. Kroes, Phys. Rev. Lett. **108**, 236104 (2012).

[46] G. Kresse and D. Joubert, Phys. Rev. B **59**, 1758 (1999).

[47] P. E. Blöchl, Phys. Rev. B **50**, 17953 (1994).

[48] G. Kresse and J. Hafner, Phys. Rev. B **47**, 558 (1993).

[49] G. Kresse and J. Hafner, Phys. Rev. B **49**, 14251 (1994).

[50] G. Kresse and J. Furthmüller, Comput. Mat. Sci. **6**, 15 (1996).

[51] G. Kresse and J. Furthmüller, Phys. Rev. B **54**, 11169 (1996).

[52] J. Klimeš, D. R. Bowler, and A. Michaelides, Phys. Rev. B **83**, 195131 (2011).

[53] J. W. Arblaster, Platinum Met. Rev. **41**, 12 (1997).

[54] J. W. Arblaster, Platinum Met. Rev. **50**, 118 (2006).

[55] H. A. Michelsen and D. J. Auerbach, J. Chem. Phys. **94**, 7502 (1991).

[56] E. B. Wilson, J. Am. Statist. Assoc. **22**, 209 (1927).

[57] G. Román-Pérez and J. M. Soler, Phys. Rev. Lett. **103**, 096102 (2009).

[58] Y. Zhang and W. Yang, Phys. Rev. Lett. **80**, 890 (1998).

[59] J. Klimeš, D. R. Bowler, and A. Michaelides, J. Phys.: Cond. Matt. **22**, 022201 (2010).

[60] G. Henkelman, B. P. Uberuaga, and H. Jónsson, J. Chem. Phys. **113**, 9901 (2000).

[61] G. Henkelman and H. Jónsson, J. Chem. Phys. **113**, 9978 (2000).

[62] S. Nave and B. Jackson, J. Chem. Phys. **130**, 054701 (2009).

[63] S. Nave, A. K. Tiwari, and B. Jackson, J. Chem. Phys. **132**, 054705 (2010).

[64] V. A. Ukraintsev and I. Harrison, Surf. Sci. **286**, L571 (1993).

[65] D. L. Meixner and S. M. George, Surf. Sci. **297**, 27 (1993).

[66] Y. Matsumoto, Y. A. Gruzdkov, K. Watanabe, and K. Sawabe, J. Chem. Phys. **105**, 4775 (1996).

[67] K. Watanabe and Y. Matsumoto, Surf. Sci. **390**, 250 (1997).

[68] A. F. Carlsson and R. J. Madix, Surf. Sci. **458**, 91 (2000).

[69] L. Chen, H. Ueta, H. Chadwick, and R. D. Beck, J. Phys. Chem. C **119**, 14499 (2015).

[70] E. Dombrowski, E. Peterson, D. Del Sesto, and A. L. Utz, Catal. Today **244**, 10 (2015).

[71] F. Viñes, Y. Lykhach, T. Staudt, M. P. A. Lorenz, C. Papp, H. P. Steinrück, J. Libuda, K. M. Neyman, and A. Görling, Chem. - Eur. J. **16**, 6530 (2010).

[72] K. Lee, E. D. Murray, L. Kong, B. I. Lundqvist, and D. C. Langreth, Phys. Rev. B **82**, 081101 (2010).